AN INTERMEDIATE-MASS BLACK HOLE IN THE GLOBULAR CLUSTER G1:
IMPROVED SIGNIFICANCE FROM NEW KECK AND HUBBLE SPACE TELESCOPE OBSERVATIONS[1]

KARL GEBHARDT[2], R. M. RICH[3], AND LUIS C. HO[4]
The Astrophysical Journal.

ABSTRACT

We present dynamical models for the massive globular cluster G1. The goal is to measure or place a significant upper limit on the mass of any central black hole. Whether or not globular clusters contain central massive black holes has important consequences for a variety of studies. We use new kinematic data obtained with Keck and new photometry from the Hubble Space Telescope. The Keck spectra allow us to obtain kinematics out to large radii that are required to pin down the mass-to-light ratio of the dynamical model and the orbital structure. The Hubble Space Telescope observations give us a factor of two better spatial resolution for the surface brightness profile. By fitting non-parametric, spherical, isotropic models we find a best-fit black hole mass of $1.7(\pm 0.3) \times 10^4 \, M_\odot$. Fully general axisymmetric orbit-based models give similar results, with a black hole mass of $1.8(\pm 0.5) \times 10^4 \, M_\odot$. The no-black hole model has $\Delta\chi^2 = 5$ (marginalized over mass-to-light ratio), implying less than 3% significance. We have taken into account any change in the mass-to-light ratio in the center due to stellar remnants. These results are consistent with our previous estimate in Gebhardt, Rich & Ho (2002), and inconsistent with the analysis of Baumgardt et al. (2003) who claim that G1 does not show evidence for a black hole. These new results make G1 the best example of a cluster that contains an intermediate-mass black hole.

Subject headings: galaxies: individual (M31) — galaxies: star clusters — globular clusters: general — globular clusters: individual (Mayall II = G1)

1. INTRODUCTION

A fundamental problem in understanding galaxy formation is knowing how supermassive black holes form and grow. The correlation between black holes and host galaxy properties (with velocity dispersion: Gebhardt et al. 2000a, 2000b; Ferrarese & Merritt 2000; or with bulge mass: Magorrian et al. 1998) highlights an intimate connection. Theoretical models are beginning to explain these correlations in detail and suggest that the supermassive black hole has significant long-ranging influence on the host galaxy (Silk & Rees 1998, Fabian 1999, Springel, Di Matteo, & Hernquist 2005, Murray, Quataert, & Thompson 2005, etc.). However, one of the main issues is understanding the seeds for the supermassive black holes, since they determine the initial mass and growth process; i.e., if intermediate-mass black holes are common then there is likely to be a significant number of merging events. Thus, the existence and number density of intermediate-mass black holes is one of the most important pieces to the puzzle.

Recent detections of active galactic nuclei (AGNs) in low-luminosity, late-type galaxies strongly suggest that intermediate-mass black holes do exist (Filippenko & Ho 2003; Barth et al. 2004; Greene & Ho 2004). Combining black hole masses estimated using the AGN luminosity and line width with stellar velocity dispersions of the host galaxies, Barth, Greene, & Ho (2005) demonstrate that the black hole mass-velocity dispersion relation extends down to $\sim 10^5 \, M_\odot$. Intermediate-mass black holes have also been invoked to explain the origin of the "ultraluminous X-ray sources" detected in nearby galaxies by Chandra (e.g., Zezas & Fabbiano 2002, Kong et al. 2005) and XMM-Newton (e.g., Foschini et al. 2002), but these measures depend on uncertain models for accretion disks, and stellar-mass black hole models may fit as well (King et al.

2001). The most robust way to measure black hole masses is through dynamics. The two claims for dynamical evidence for intermediate-mass black holes are for G1 in M31 (Gebhardt, Rich, & Ho 2002) and M15 (van der Marel et al. 2002; Gerssen et al. 2002), both of which have been challenged by Baumgardt et al. (2003a,b). Here we present analysis of G1 and de Zeeuw et al. (2005) present new analysis for M15.

In Gebhardt, Rich & Ho (2002), we present data and dynamical models for G1 that suggest the existence of a $2 \times 10^4 \, M_\odot$ black hole. Subsequently, Baumgardt et al. (2003b) compare our data to their dynamical models and argue that a model with no black hole fits as well. In this paper, new data and analysis strongly support the black hole interpretation. Furthermore, we argue that the Baumgardt analysis is fundamentally inconclusive since they use a simplified comparison between data and theory. Thus, even with the data as presented in Gebhardt, Rich & Ho, the black hole interpretation is preferred, but the new data presented here give yet stronger evidence.

First we outline the appropriate techniques that should be used to measure black hole masses, and discuss why our previous analysis and modeling are preferred. We then provide new data and results which strengthen the black hole interpretation.

2. MEASURING BLACK HOLE MASSES

The history of supermassive black hole studies is the subject of many reviews (e.g., Kormendy & Richstone 1995, Kormendy & Gebhardt 2001, Ho 1999). Here we concentrate on the main kinematic requirements for accurate measurements and the modeling techniques for optimal constraints of central black holes. It has been know since Binney & Mamon (1982) and Tonry (1983) that using the second moment of the velocity profile alone to measure the mass profile can lead to

---

[2] Astronomy Department, University of Texas, Austin, TX 78723; gebhardt@astro.as.utexas.edu

[3] UCLA, Physics and Astronomy Department, Math-Sciences 8979, Los Angeles CA 90095-1562; rmr@astro.ucla.edu

[4] The Observatories of the Carnegie Institution of Washington, 813 Santa Barbara St., Pasadena, CA 91101; lho@ociw.edu

substantially biased results. The problem is that the velocity anisotropies of the stars trade off with the shape of the potential to create a variety of profiles for the second moment. Thus, any assumption about the stellar orbital distribution must be explored carefully. One, however, can get a handle on the orbital distribution by exploiting at least the first moment of the velocity distribution (i.e., the velocity) along with the velocity dispersion, and, more importantly, higher-order terms. Van der Marel (1991) demonstrates the power of using additional information to extract the orbital structure. The most information that can be extracted from any spectral dataset results from using the full line-of-sight velocity distribution (LOSVD) at as many positions in the object as possible. Using velocity dispersion data alone (or even the second moment) cannot overcome the degeneracy with the orbital structure. Magorrian et al. (1998) demonstrate how sensitive the estimate of the black hole mass is to changes in the assumed anisotropy when using the second moment alone. The current state of the art is to use the full velocity profile when possible.

The dynamical modeling is just as important as the data analysis, since any assumptions in the models will greatly bias the orbital structure and hence the mass profile. Gebhardt (2004) reviews the classes of models that have been used to measure the central potential. One must use orbit-based models in order to include degeneracies with the stellar orbital structure. These are now commonplace and standard (Gebhardt et al. 2000c, 2003; Cappellari et al. 2003; Krajnovic et al. 2005). These models provide the most freedom for the distribution function in axisymmetric systems (triaxial models are now in development—see van de Ven et al. 2004—and will soon be as common). Alternatively, N-body simulations provide just as general results in terms of priors on the distribution function. N-body simulations that reach the size of realistic clusters and galactic nuclei will therefore be another tool for the study of central black holes. Gebhardt, Rich & Ho (2003) use orbit-based models and Baumgardt et al. (2003b) use N-body simulations to constrain the central black hole mass. The difference in the two results is due to *both* how they include the kinematics and the theoretical comparison. We discuss both of these.

2.1. *Velocity Dispersion is Not Enough*

First, Gebhardt, Rich & Ho model the full velocity profile (as is done in this paper) whereas Baumgardt et al. only use the second moment (they actually plot the first moment but never use it in their χ^2 measurements). It is known that the second moment alone is not adequate in general. However, for an object like G1 where the sphere of influence of the black hole is barely resolved, it is crucial to use all of the kinematic information. Specifically, the signature of the black hole is one of increasing the wings of the velocity profile near the center. The extreme consequence is to cause exponential tails in the central velocity profile, but this would only be seen in the best spatially resolved cases (as demonstrated for M87 by van der Marel 1994). For G1, if Gebhardt, Rich & Ho had used the second moment alone to constrain the black hole mass they, too, would have argued that the no-black hole model is acceptable. In fact, the no-black hole model of Gebhardt, Rich & Ho provides a better fit to the second moment than the no-black hole model of Baumgardt et al. Yet, ironically, Baumgardt et al. argue for no black hole and we argue for a black hole. The difference is because we use more information than used by Baumgardt et al. Unfortunately, the N-body simulations do not have enough particles to

measure a reliable velocity profile. So the only recourse that Baumgardt et al. have is to use the second moment (even the first moment is difficult to measure due to the shot noise in the N-body simulations). This leaves us in the unfortunate situation where we cannot use the same dataset for comparison. However, we strongly argue that by not using the full velocity profile one is severely limiting the generality of the results and potentially introducing biases.

2.2. *Parameter Estimation vs. Hypothesis Testing*

Second, Gebhardt, Rich & Ho compare black hole and no-black hole models in a differential sense, whereas Baumgardt et al. use an absolute comparison between their no-black hole model and our data. In order to determine whether inclusion of a black hole provides a better fit, one must use a differential comparison. This issue is discussed in Gebhardt et al. (2000c), but we summarize the main points here. The two analyses highlight the difference between parameter estimation (our analysis) and hypothesis testing (Baumgardt et al. analysis). Hypothesis testing is the most base level analysis that has very little power to discriminate whether a black hole exists. For example, if a kinematic dataset has a significant amount of data outside of the black hole sphere of influence, the majority of a goodness-of-fit statistic is dominated by regions that cannot discriminate whether a black hole is present. Thus, even if a central kinematic measurement is not in agreement, the hypothesis test will de-weight that sole deviation. In parameter estimation, a difference test (i.e., using $\Delta\chi^2$), directly shows the effect of including a black hole, and is therefore not sensitive to the amount of data at large radii. Since the black hole in G1 has such a small sphere of influence it is imperative to use a differential analysis. The main problem with the Baumgardt et al. analysis is that they cannot run realistic N-body simulations that include a black hole (they have too few particles), so they are forced to perform a hypothesis test. Thus, their result is severely compromised to the point where one can draw very little meaning to their comparison to the G1 data.

2.3. *Other Issues*

Above are the two main concerns, but additional worries about the N-body simulations exist. Other issues are the scaling of results to realistic clusters and their initial hidden assumptions. For G1, even for the largest N-body simulation, they must scale the mass by a factor of over 150. It has not been demonstrated that such an extreme scaling produces accurate results, especially near the cluster center. In fact, Baumgardt (2001) demonstrate how difficult it is to scale even simple single-mass models. For this resolution, we have to wait until the simulations become more sophisticated. Another issue with the N-body simulations is the influence of binary stars. Baumgardt et al. also do not include binary stars, which are likely to dominate the core dynamics (Fregeau et al. 2003), and thus change the M/L profile in the N-body simulations

Another potentially important concern is how stellar remnants are handled. The two components that need to be understood are the neutron star retention factor and the present-day mass profile for white dwarfs. The neutron star retention factor appears not to be a serious issue anymore since the recent N-body simulations from Baumgardt et al. use very little retention. The contribution from neutron stars to the central mass profile is likely to be very small. This is not true of older simulations (e.g., Dull et al. 1997), so one must be aware of these

differences. We know, however, that clusters do contain pulsars, so the retention factor is larger than zero. The best estimates place it between 5 and 15% (Pfahl et al. 2002). Recent results from Heinke et al. (2005) using Chandra show that 47Tuc's neutron star population is consistent with a very low retention fraction. A more important issue is the initial-to-final mass relation for white dwarfs. The remnants that have the most influence on the central structure are the heavy white dwarfs. Nearly all N-body simulations use the stellar evolutionary models of Hurley, Pols, & Tout (2000). For the initial-to-final mass relation, they use an empirical fit to the data of Jeffries (1997) for 4 white dwarfs in the same cluster. Both recent observational and theoretical results, however, give a significantly different relation. The theoretical models of Weidemann (2000) or the observations of Kalirai et al. (2005) show that the final mass of the heavy white dwarf is smaller by about 0.2 solar mass compared to Hurley et al.'s estimate. Kalirai et al. also find a slight, but noisy, dependence on metallicity, with lower metallicity possibly producing heavier remnants. For a cluster like G1, the smaller masses for the white dwarfs will have an important effect on dynamical friction timescales, and thus we should not expect as large a contribution to the central mass from them as Baumgardt et al. suggest. New N-body simulations should include the most up-to-date initial-to-final mass relation for white dwarfs in order to provide realistic results.

The final mass of the white dwarfs do not affect our analysis as much as in the N-body simulations. The orbit-based models rely on having an estimate of the mass-to-light (M/L) ratio in order to provide an input gravitational potential. The N-body simulations of G1 from Baumgardt et al. (2003) show that the M/L profile of G1 near the center is at least constant and possibly even decreasing. Given the age around 13 Gyr for G1 (Meylan et al. 2001) and a turn-off mass around 0.9 $M_\odot$, massive giant stars tend to dominate the light in the core; even though there are remnants in the core, the combined M/L tends to remain constant. The models of Baumgardt et al. actually show a slight drop in the M/L near the center of G1. In our analysis we assume a constant M/L ratio. We have tried a variety of realistic expectations for the M/L variation (as in Gebhardt, Rich & Ho) and all models strongly support the existence of a central black hole.

We now turn to results from newer data and analysis on G1, but argue that the black hole as presented in Gebhardt, Rich & Ho is robust.

3. DATA

One of the larger uncertainties in the previous dynamical models is the comparison with kinematics at large radii. The overall mass-to-light ratio is extremely important since it helps to set the scale at small radii where the influence of the black hole is seen. Furthermore, orbit-based models require some knowledge of large-radii kinematics since the models need to constrain the influence of orbits with highly radial motion. For example, a central black hole can easily be disguised if one includes a large amount of radial orbits. However, in this case, the radial orbits will have a large effect at large radii, causing a significant drop in the projected dispersion there. Thus, by having large-radii kinematics, one can limit this effect. In our previous analysis, we relied on a signal-aperture measurement from the ground-based spectroscopy of Djorgovski et al. (1997) to provide most of the large-radii leverage. In order to improve upon this, we obtained high signal-to-noise (S/N) spectra from

Keck.

The other issue is that the central light profile was not very well determined in the previous analysis. The previous HST imaging suffered from saturation, no dithering, and coarser resolution. We have obtained improved (*HST*) imaging, which we present below.
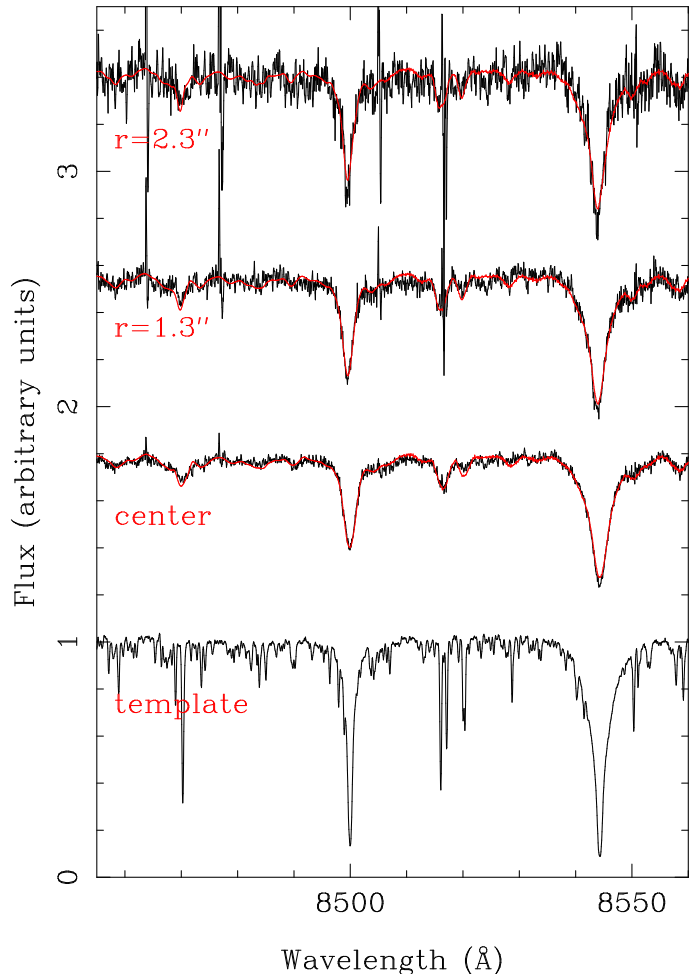

FIG. 1.— Keck spectra and fits for G1. The wavelength range includes two of the Calcium triplet lines (and some weaker lines). The bottom spectrum is the template used for the estimation of the velocity profile. The upper spectra come from different radii. The noisy lines are the data, and the red lines are the template convolved with the velocity profiles.

3.1. *Keck Spectra*

The Keck data were obtained on October 19, 2003 using the high-resolution spectrograph HIRES. We observed a total of 2.8 hours. We used a 1.72″ slit and the 14″-long D4 decker. The spectra run from 6390 to 8770 Å. This setup produces an instrumental resolving power of R=23,000, or resolution of 13 km s^{-1} (FWHM) at 8500Å, which is ideal for the velocity dispersion of G1 (10–30 km s^{-1}). The spatial scale in the cross-dispersed direction is 0.191″ per unbinned pixel. We binned by two in the cross dispersed direction since we are mainly concerned about large-radii kinematics. Around 8500Å the wavelength scale is about 0.0626Å per pixel in the dispersed direction. The FWHM of the seeing during the observations was about 1.2″.

We used the reduction package MAKEE (written by Tom Barlow) for the data analysis. We compared these results to our own reduction procedure and found no significant differences. However, the ease of use of MAKEE make it an excellent and

ideal package. The MAKEE package performs standard flattening, traces and extraction. Since we are interested in spatial information, we extracted spectra along various radii. With the 14″ slit and the size of G1 (half-light radius around 1.5″), we always had sky in part of the slit that we used to subtract from the data. Our furthest radial bin runs from 3″–4.6″, leaving us with 2.5″ for sky estimation. We checked whether residual light from G1 contaminates the sky by running the kinematic extraction with and without the sky subtraction. While the results with no sky subtraction give substantially worse results, the kinematics are qualitatively the same. Thus, the sky appears to be well measured and subtracted.

Figure 1 presents spectra at three different radii in G1. The bottom spectrum is a template star. It is clear that the Calcium triplet lines at all radii are easily resolved with this setup. The S/N in the central spectrum is 55 per extracted pixel (corresponding to 0.0626Å by 0.382″). At our largest radii, S/N=6.7 per extracted pixel (0.0626Å by 1.6″). We had five individual exposures for G1. Each is extracted separately and the continuum divided out before making combined spectra.

We use the kinematic extraction technique outlined in Gebhardt et al. (2000c) and Pinkney et al. (2003). This technique provides a non-parametric estimate of the LOSVD, which is used directly in the models. Traditionally, one reports the moments of the velocity profile. Below we calculate the moments, but keep in mind that these moments are not used in the models but instead the full LOSVD. The shape of the LOSVD provides important information about the orbital structure and even the black hole mass; it is important to include the full velocity profile when making dynamical models. Table 1 presents the first four moments of the velocity profile from the ground-based kinematics. These are the velocity, velocity dispersion, H3 and H4. H3 and H4 represent diviations from a Gaussian using a Gauss-Hermite polynomial. H3 is similar to skewness and H4 similar to kurtosis. Van der Marel & Franx (1993) and Bender et al. (1994) provide detailed discussion of the Gauss-Hermite expansion. These first four moments are determined directly from our non-parametric estimate of the LOSVD. We only present the symmetrized version of the kinematics. We symmetrize by fitting spectra at the same radii on opposite sides of the cluster simultaneously to the LOSVD; however, the LOSVD is appropriately flipped about zero velocity from one side compared to the other, which is the expected configuration for an axisymmetric system. The uncertainties in Table 1 have been symmetrized; our fitting procedure includes the actual uncertainty distribution, but since this distribution is nearly symmetric we present only symmetrized uncertainties in the Table. For both the STIS and Keck data the width of the extraction window varies with radius, and the uncertainties at each point depends on the surface brightness and extraction width.

We observed four different template stars: two K4III stars, one K0III, and one M1III. All templates give nearly identical results for the kinematics. The rms of the kinematic parameters for the four templates scatter within the 1 σ uncertainties presented in Table 1. Our final results are based on using just one K4III star but would remain unchanged with any of the template. The Calcium triplet region is therefore quite robust to template variations, as discussed in Barth, Ho, & Sargent (2002).

We reanalyse the STIS spectra presented in Gebhardt, Rich & Ho (2002). The differences mainly include a different re-sampling and combining of the individual spectra and a new extraction of the LOSVD. Given that the instrumental resolution of STIS is approaching the dispersion of G1 near the center, one needs to take this into account carefully. Our re-analysis is very similar to our published results, with the dispersions being about 3% smaller in the center and 9% smaller at the largest radii. These changes are well within the quoted uncertainties. The differences at large radii (1″ for STIS) make essentially no difference in the dynamical modeling since they have large uncertainties, and the high S/N ground-based spectra dominate the fits there. Thus, the new analysis changes none of the results but should be used for any future modeling. Table 1 presents the moments of the LOSVDs for the STIS spectra.
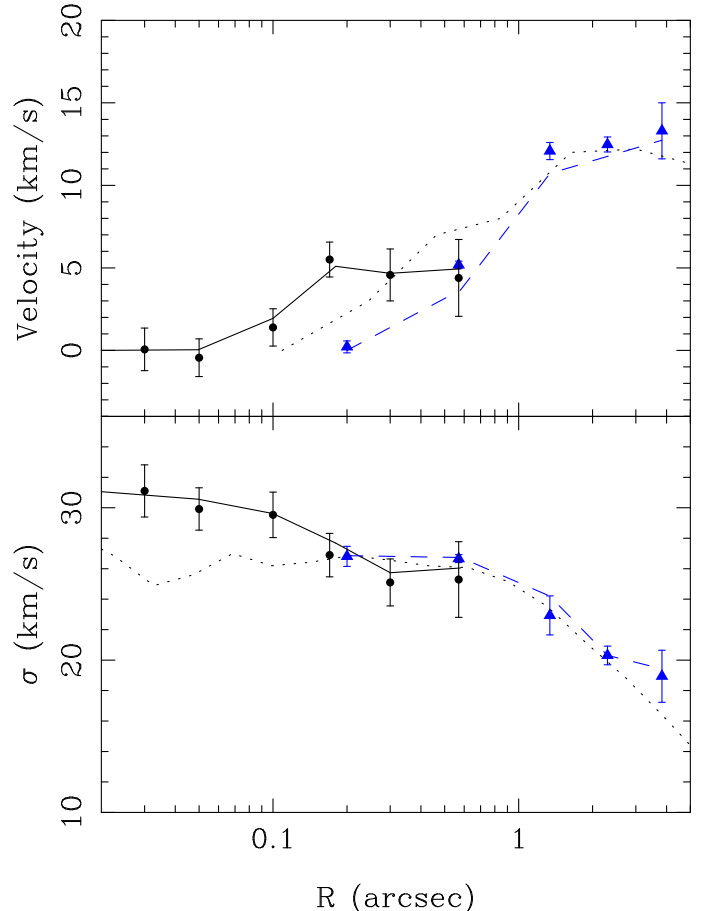

FIG. 2.— Projected velocity (top) and dispersion (bottom) for G1 including the Keck (blue triangles) and STIS (black circles) data. The STIS data have been re-analyzed since Gebhardt et al. (2002). The data have been folded about the center. For both sets of data we plot the symmetrized version. The solid and dashed lines represents the kinematics from our best-fit model (including the black hole) for the STIS and Keck data, respectively. Our model presented here includes the increase in M/L at large radii. The dotted lines are the kinematics from Baumgardt et al. (2003b) no-black hole model, which clearly is low in the central regions (discussed in Section 5).

Figure 2 presents the first two moments (velocity and velocity dispersion) of the velocity profile for the STIS and Keck spectra. The agreement between the STIS and Keck data is excellent. At small radii, the velocity profiles disagree due to seeing in the Keck data. At large radii, G1 has substantial rotation. At 4″ v/σ is around 0.7, which makes it one of the fastest rotators ever seen for a globular cluster. ω Cen has the highest v/σ measured for a Galactic globular cluster, with $v/\sigma = 0.3$ (van de Ven et al. 2005).
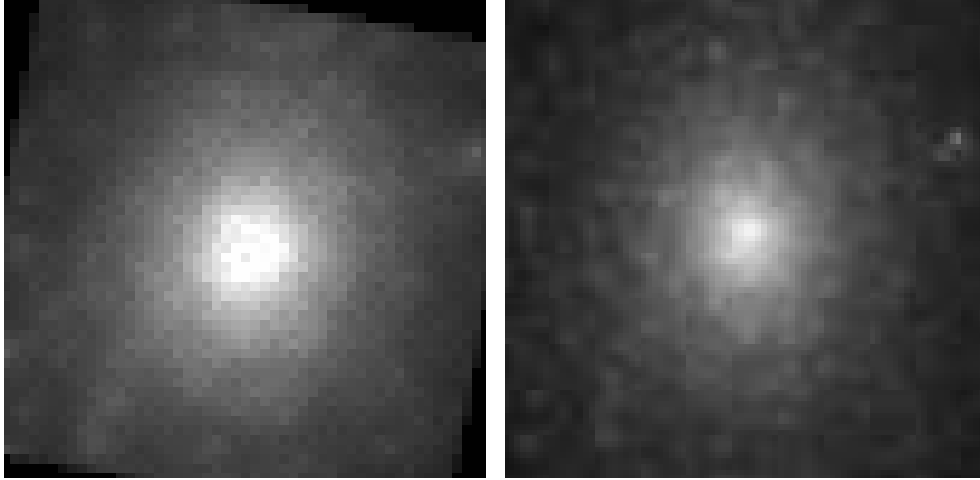
FIG. 3.— HST observations of the central 2.3″ diameter using the PC/F555W on WFPC2 (left) and using HRC/F555W on ACS (right). The HRC image is deconvolved. The central structure is clearly more detailed in the HRC image, allowing us to see the effects of individual bright giant stars.

3.2. *HST/ACS Observations*

We took HST images of G1 with the High-resolution Camera (HRC) on the ACS. The total integration is 41 minutes in the filter F555W over six exposures at three positions. Figure 3 shows the central 2.3″ with WFPC2 (obtained from the HST archive) and our deconvolved ACS/HRC image.

The individual exposures are shifted with linear interpolation and combined with a biweight estimator (Beers, Flynn, & Gebhardt 1990). We deconvolve using 140 Lucy-Richardson iterations (Lucy 1974). The ACS/HRC PSF is taken from the HST handbook and uses Tiny Tim. We tried different numbers of Lucy-Richardson iterations and anything over 20 produces nearly identical results. The ACS pipeline produces a drizzled image as well; we find no significant differences between our image and the drizzled image. For the surface brightness profile, we determine the central location and scatter of the pixels in ellipses centered on the cluster. We use an ellipticity constant with radius. The central location and scatter are determined from the biweight estimators. The center determination is an important aspect for the surface brightness profile. In G1, we are spatially resolving the brightest giants, and bright stars near the center can skew its determination. Therefore, the center measured from the isophotes at larger radii provide a more accurate determination. In fact, the center measured from the outer isophotes is 1.2 HRC pixels (1.2x0.0266″=0.03″) different from the brightest pixel near the center. If we use the center as determined by the brightest pixel in the central parts of the image, the surface brightness is slightly brighter than using our best-measured center. This increase provides more stellar mass there and makes the black hole mass determination slightly less significant. In the subsequent analysis, the $\Delta\chi^2$ between the no-mass black hole and the best fit changes from 5 to 4.2. However, the bright spot near the center of the image appears to be a bright star, as the isophotal analysis suggests. Figure 4 plots the surface brightness profile for G1. We include our previous determination using WFPC2 images. We can obtain the exact WFPC2 surface brightness profile by using a center as defined by the brightest pixel, indicating that our old WFPC2 analysis was influenced by not being able to resolve the central bright star. HRC images give us a factor of two improved spatial resolution.
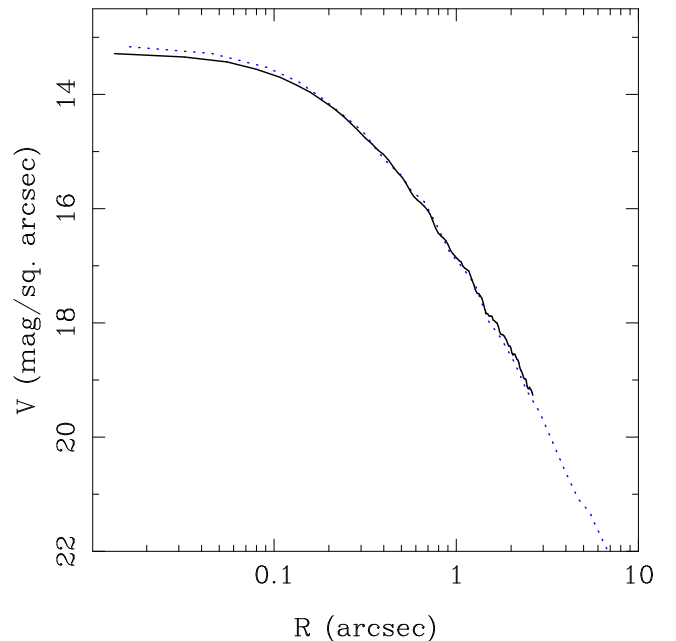

FIG. 4.— Surface brightness profiles for G1. The blue dotted line is from the WFPC2 data that were used in Gebhardt et al. (2002). The black solid line is from the deconvolved ACS/HRC image, and is used in the subsequent analysis. The improved spatial resolution allowed us to better center the cluster and avoid contribution from a bright star, which causes the decrease in the central brightness seen in the HRC profile compared to the WFPC2 profile.

4. MODELS

There are a variety of dynamical models that are available. We model G1 both with isotropic, non-parametric models, and with fully general orbit-based models. Baumgardt et al. (2003b) provide a dynamical model for G1 that is very different from our models. They use evolutionary models and find the best fit to the data by comparing N-body simulations with varying initial conditions. Thus, they have a robust evolutionary model but are limited in their comparison by their particular N-body runs (i.e., initial conditions, number of particles, etc.). Our models are static equilibrium models, and we do not follow the evolution. However, the orbit-based models allow us to modify the distribution function in order to get the best match to the data while still being a solution to the Jeans equations. Thus these orbit-based models have significantly more freedom
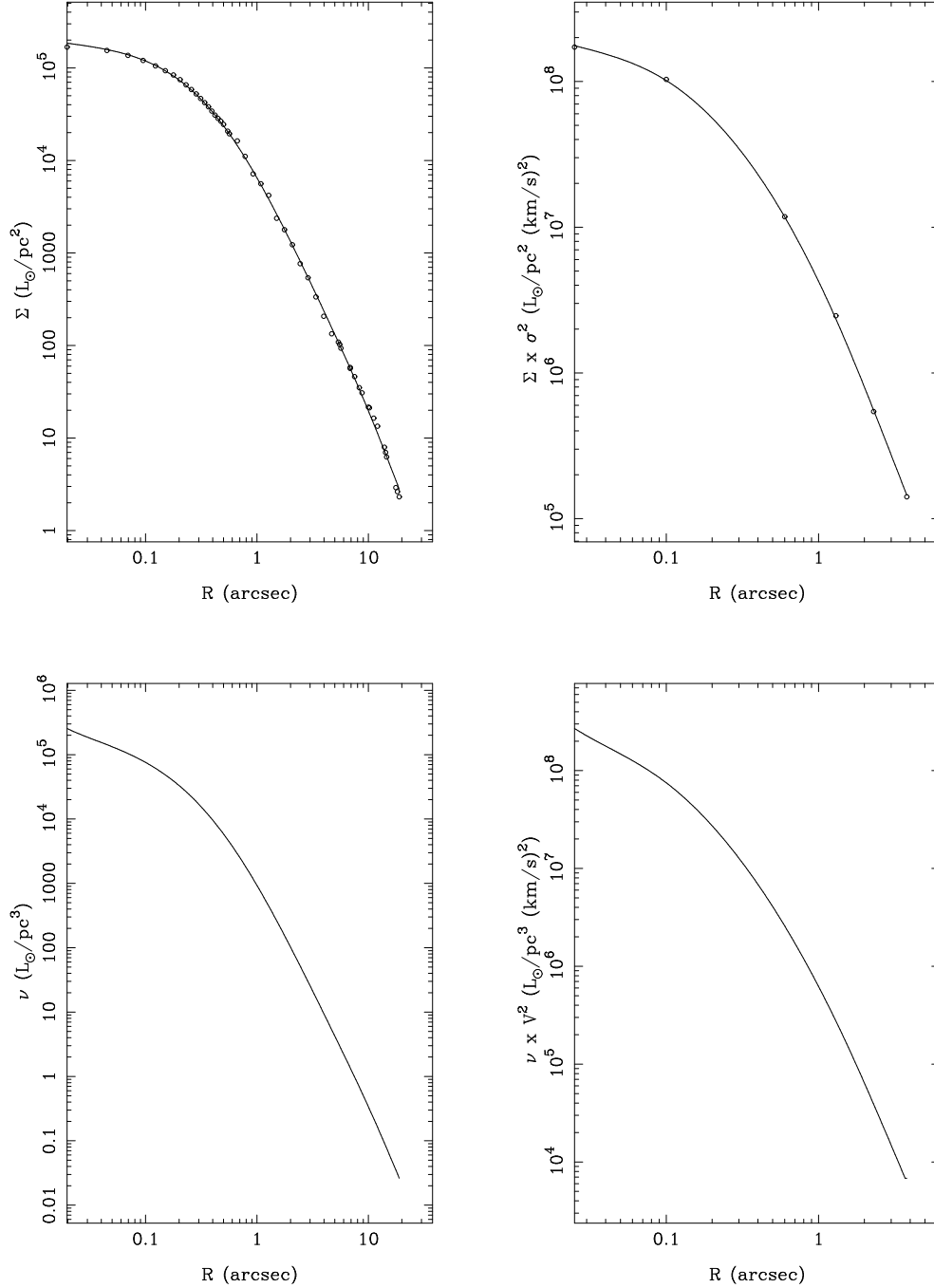
FIG. 5.— The left panels are the projected and internal light profiles for G1, where we have used a non-parametric deprojection. The right panels are the projected and internal values for the light profile multiplied by the second moment of the velocity distribution. For the projected velocity distribution we are using $\sigma^2 = v^2 + \sigma_d^2$.

and produce a more general result.

However, before discussing the orbit-based models, we model G1 as an isotropic spherical system. While this is not the case for G1, since it is flattened with axis ratio 0.75 (as measured from our image), it does provide a good comparison. Furthermore, the short dynamical timescales in the central regions of G1 (the central relaxation time is about 2×10^8 years) may cause the orbits to be nearly isotropic. Since our goal is to constrain the central mass profile and the rotation is a small component of the velocity dispersion near the center, we make only a small error by assuming isotropy there. At large radii, however, this assumption will likely break down due to the large

rotation and long relaxation times.

4.1. *Non-Parametric Models*

We use the non-parametric models as discussed in Gebhardt & Fisher (1994). Given a surface brightness profile and a velocity dispersion profile, the spherical Jeans equation uniquely determines the mass density profile (and hence the M/L profile) assuming isotropy. This is a straightforward exercise that we demonstrate in Figures 5 and 6. Through an Abel deprojection, the surface brightness profile uniquely determines the luminosity density. Similarly, the surface brightness times the projected velocity dispersion determines the luminosity density
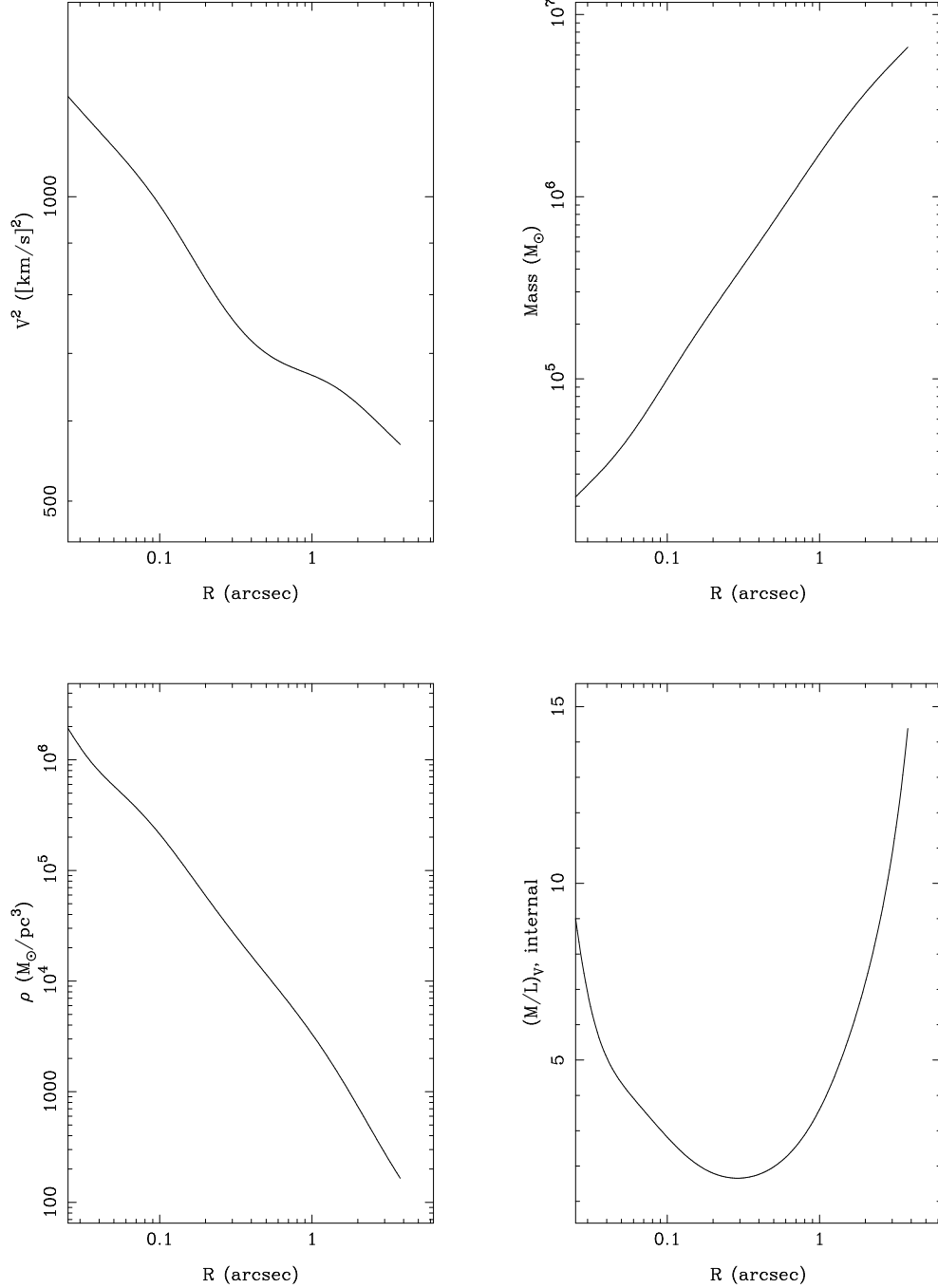
FIG. 6.— Internal dynamics for G1. The top left is the square of the second moment of the internal velocity distribution. The top right is the enclosed mass as a function of radius. The bottom left is the mass density, and the bottom right is the internal mass-to-light ratio.

times the internal (3-D) velocity dispersion. One must use some degree of smoothing to represent these profiles since the Abel deprojection involves a derivative. This is discussed in detail in Gebhardt et al. (1996), and we using Generalized Cross-Validation (Wahba 1990) to determine the best-fit smoothing parameters. We have also tried different smoothings and find very little effect on the main conclusions.

One then measures the internal velocity by dividing out of the luminosity density (i.e., dividing the curve in the bottom-left panel in Figure 5 into the one in the bottom-right panel). The top-left panel in Figure 6 shows the internal velocity squared versus radius. It is then straightforward to determine the en-

closed mass and M/L profiles.

The bottom-right panel of Figure 6 shows the M/L profile versus radius. The two obvious features are the increase at large radii and the increase at small radii. The increase at large radii is expected since that region is dominated by low-mass stars. Indeed, Baumgardt et al. (2003b) find a similar result in their N-body models. However, the increase at small radii is not expected from the evolutionary models with no black hole. The M/L increases by about a factor of 3.5 from the lowest point. G1 has a turn-off mass around one solar mass. Since the average mass of the stars in the cluster should be around 0.6 solar masses, the one-solar mass stars, as well as the stellar remnants

of neutron stars and stellar-mass black holes, will sink into the center by dynamical friction. However, since the turn-off stars and giants are so bright, they tend to drive the M/L to smaller values. The stellar remnants drive the M/L to high values, and the resulting combined M/L profile is to remain relatively flat. In fact, Baumgardt et al. argue that the central M/L should be slightly depressed compared to the global M/L profile.

Thus, the increase in the M/L profile at small radii is not consistent with normal stellar evolution without a central black hole. We can estimate the mass of the central black hole from the top-right panel in Figure 6, the enclosed mass profile. In the central bin (radius=0.025″) there is 2×10^4 solar masses of material. The contribution from stars and remnants at these radii is small; we estimate the stellar mass by using the total light inside of 0.025″, which is about $900\,L_\odot$, multiplied by the M/L of 2.8, giving $0.3 \times 10^4\,M_\odot$. Thus, the best estimate for the black hole mass is about $1.7 \times 10^4\,M_\odot$. Uncertainties come from the noise on the surface brightness and velocity dispersion profiles, and are around $0.3 \times 10^4\,M_\odot$, but these only represent measurement uncertainties and do not take into account potential assumption biases.
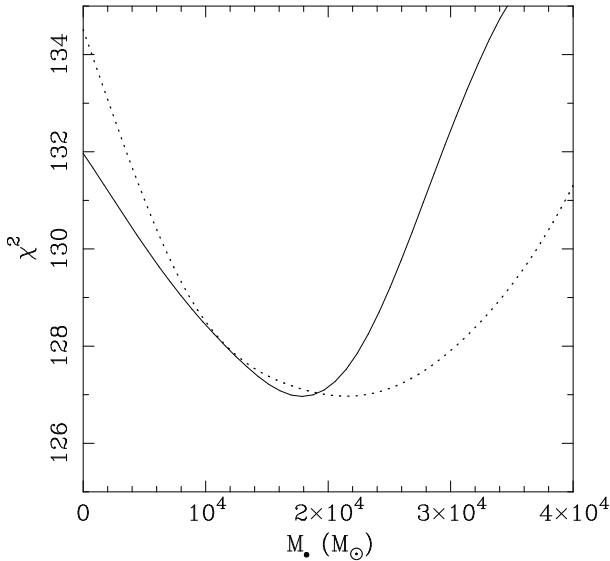

FIG. 7.— χ^2 versus black hole mass marginalized over mass-to-light ratio. The solid line represents the constant M/L model, while the dashed line has an M/L profile that rises at large radii according to Figure 6. The difference in χ^2 between the no-black hole mass and the best fit is 5 for a constant M/L, which implies a significance of over 97%. The case with a varying M/L shows an even higher $\Delta\chi^2$ with the no-black hole model, and allows for a higher mass black hole. We add 37 to the χ^2 for the varying M/L model, since it is a better fit to the data.

4.2. *Orbit-Based Models*

We use fully general axisymmetric orbit-based models. These are described in Gebhardt et al. (2000c, 2003), Thomas et al. (2004), and Richstone et al. (2005). The models do not rely on a specified form for the distribution function. Thus, for an axisymmetric system, these models provide the most general solution. The models require an input potential, in which we run a set of stellar orbits covering the available phase space. We find a non-negative set of orbital weights that best matches both the photometry and kinematics to provide an overall χ^2 fit. We vary the central black hole mass and refit.

The orbit-based models store the kinematic and photometric results in both spatial and velocity bins. For G1, we use 12 radial, 4 angular, and 13 velocity bins. The number of bins is

chosen to match the kinematic extraction windows as well as possible. The data consist of the seven different STIS positions along a position angle of 25° up from the major axis and the ground-based data along the major axis. The point-spread function for both *HST* and ground-based observations are included directly into the models, as well as the slit size. The program matches the luminosity density everywhere throughout the cluster to better than 0.5%. The quality of the fit is determined from the match to the velocity profiles. We use about 4800 orbits to sample the phase space. The orbit number is driven by the number of spatial bins used in the models (as described in Richstone et al. 2005). For the binning used for G1, the minimum number of orbits is around 2400.

Figures 7 and 8 show the results for the models. Figure 7 plots the one-dimensional χ^2 versus black hole mass, marginalized over M/L ratio. Figure 8 plots the two-dimensional χ^2 contours as a function of black hole mass and M/L ratio. For these models we use a constant M/L ratio. The best-fit black hole mass is $1.8(\pm 0.5) \times 10^4 M_\odot$. The uncertainty represents the span of $\Delta\chi^2 = 1$ from the minimum value, which is the 1 σ band for one degree of freedom (since we marginalize over M/L).
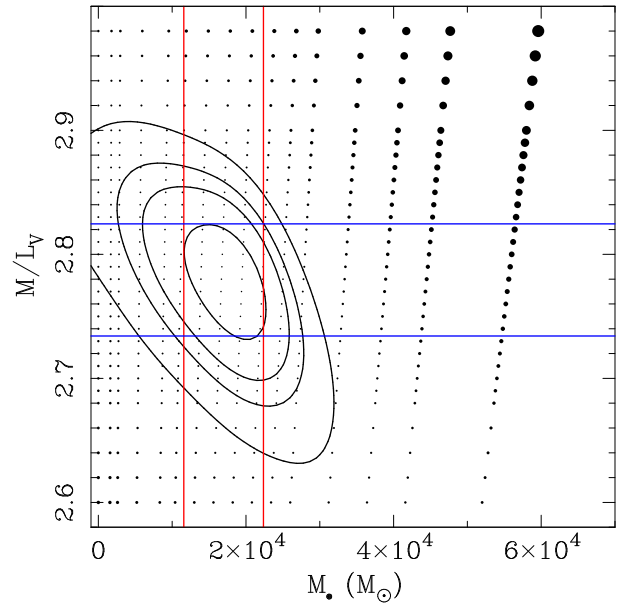

FIG. 8.— Two-dimensional χ^2 versus black hole mass and mass-to-light ratio. Each point represents a model, and the size of the point reflects the value of $\Delta\chi^2$. The contours refer to $\Delta\chi^2 = 1.0, 2.71, 4.0, 6.63$, and so corresponds to one degree of freedom confidence levels of 68, 90, 95, and 99%. The best-fit black hole mass is $1.8(\pm 0.5) \times 10^4 M_\odot$.

The contours shown in Figs. 7 and 8 result from a smoothed version of the χ^2 values. We apply a two-dimensional smoothing spline (Generalized Cross-Validation: Wahba 1990) to the χ^2 distribution with black hole mass and M/L. In this way, we obtain more realistic uncertainties by interpolating between points with a smooth function. The actual χ^2 values lie very close to the smooth curves seen in Fig. 7, and have insignificant differences for the best-fit black hole mass. The smoothing is designed to minimize shot noise in the model values due to grid effects and limited orbit number.

The M/L ratio of G1 is, however, not constant. At large radii the M/L ratio increases, but at small radii the stellar M/L ratio is nearly constant. Thus, we are using an incorrect profile. We include a varying M/L ratio by having it increase at large radii according to the profile in Figure 6 (bottom right), but leaving

it constant at small radii (as expected from the simulations of Baumgardt et al. 2003). The one-dimensional χ^2 is shown in Fig. 7. The two-dimensional χ^2 is not shown in Fig. 8 but demonstrates the same result as Fig. 7. With the varying M/L profile, the best-fit black hole mass is $2.1 \pm 0.6 \times 10^4 M_\odot$. The χ^2 values are significantly lower—by $\Delta\chi^2 = 37$—as expected since the large-radii data show an increase in the dispersion compared to the constant M/L model.

It is clear by the change in χ^2 that the varying M/L model is a better fit. However, the M/L that we choose results from an isotropic analysis and may not be appropriate. Since we are not exploring a full range of M/L profiles, we choose a conservative approach for an estimate of the black hole mass by quoting the constant M/L results. The M/L may increase at large radii due to anisotropy, a change in the stellar population, or even the inclusion of dark matter. Globular clusters are thought to have low-mass stars at large radii due to mass segregation, which is the obvious way in which the M/L would increase. The increase seen in the isotropic models is large—around a factor of six—for what is seen in other globular clusters, so additional explanations from mass segregation may be in order. We only have kinematics along one axis for G1, so a full analysis of the M/L profile from our data likely will be inconclusive. Additional observations of large-radii kinematics of G1 and other massive clusters are required in order to understand the M/L profile.

5. DISCUSSION AND CONCLUSIONS

Using either a simple non-parametric model or a fully general axisymmetric model, we find a best-fit black hole mass in G1 of $1.8(\pm 0.5) \times 10^4 M_\odot$. This mass is consistent with our previously published result (Gebhardt, Rich & Ho 2002). This result is not consistent with the conclusion of Baumgardt et al. (2003b). There are multiple reason for the differences. First and most obviously, we are using a significantly improved dataset. The Keck spectra allow us to determine the M/L significantly better than we could do before. The improved HST imaging allows us to constrain the stellar light in the central $0.1''$, which was not possible with the older WFPC2 data. Both of these data improvements should have an important consequence on the comparison with Baumgardt et al. In fact, in Figure 2 we plot the best-fit model of Baumgardt et al. There is a clear trend for the central dispersions and velocities in the data to be higher than the values in the model. The increase is consistent with the black hole mass that we measure. However, this comparison is not exactly fair since the Baumgardt et al. model was designed to match the older STIS and ground-based data for G1. It would be important to compare these newer data to their models again, but it does appear at this stage that their models with no black hole will fail to match the data. The other reasons for the difference between the two groups are our use of the full LOSVD compared to the moments and the fact that we compare black hole models in a differential sense.

There are indications that the black hole mass versus velocity dispersion correlation for galaxies extends down to low masses and dispersions. Barth, Greene, & Ho (2005) provide the most recent dataset that demonstrates this extension. However, their results are based on estimating the black hole mass from broad-line physics, which is well-calibrated for higher-mass black holes but not for low-mass black holes. The black hole mass

that we present here for G1 is based on dynamics, which should be on much more solid footing. In fact, given G1's integrated velocity dispersion of 25 km s^{-1}, the expected black hole mass from the Tremaine et al. (2002) relation is $2.3 \times 10^4 M_\odot$. Our measured mass of $1.8(\pm 0.5) \times 10^4 M_\odot$ implies that the $M_\bullet - \sigma$ relation can be extrapolated to these small systems.

G1 may not be a globular cluster but instead the stripped nucleus of a dwarf galaxy. Meylan et al. (2001) suggest G1 is similar to the nucleus of NGC 205, and Ferguson et al. (2002, 2005) and Ibata et al. (2005) report evidence for a disrupted galaxy that is centered on G1, although there is no evidence for a discrete system. In addition, Reitzel, Guhathakurta, & Rich (2004) find no evidence as well for a separate system from their spectroscopic study of stars in the vicinity of G1. Nevertheless, compared to globular clusters, G1 would have the highest measured velocity dispersion (cf. clusters in NGC 5128; Martini & Ho 2004) and highest v$/\sigma$. The high rotation seen in G1 may be a further clue to its history since it is difficult to create such large rotation with an isolated cluster (Baumgardt et al. 2003b). Thus, it seems plausible that G1 is a stripped nucleus. There are at least two other dwarf galaxies that have AGN evidence suggestive of an intermediate-mass black hole. These are NGC 4395 (Filippenko & Ho 2003) and POX 52 (Barth et al. 2004). Further support of dwarf galaxies with black holes come from the study of Greene & Ho (2004; see also Barth, Greene, & Ho 2005). Given our dynamical evidence for a black hole in G1 and that it may be an accreted dwarf galaxy, there is mounting support for the picture that some dwarfs contain black holes. Since small galaxies accrete onto larger galaxies in the hierarchical growth of structure, there must be observable consequences for having numerous intermediate-mass black holes sinking into the centers of large galaxies.

However, it does not appear that all nuclei of small galaxies contain black holes. M33's nucleus has an upper limit of $1500 M_\odot$ (Gebhardt et al. 2001). There are no obvious differences between the surface brightness profiles between G1 and that of the nucleus of M33 (M33 has a slightly higher central density), but the difference is dramatic in the velocity dispersion profile; the dispersion of M33's nucleus drops toward the center while that of G1 rises. It is clear that the data for G1, compared to that of M33's nucleus, would favor the presence of a black hole, but it is not obvious why the two systems evidently have experienced such a different evolutionary history. We clearly need to address the issue of black holes in small galaxies with a significantly larger sample.

REFERENCES

Barth, A., Greene, J., & Ho, L.C. 2005, ApJ, 619, L151
Barth, A., Ho, L.C., Rutledge, R., & Sargent, W. 2004, ApJ, 607, 90
Barth, A., Ho, L.C., & Sargent, W. 2002, AJ, 124, 2607
Baumgardt, H. 2001, MNRAS, 325, 1323
Baumgardt, H., Hut, P., Makino, J., McMillan, S., & Portegies Zwart, S. 2003a, ApJ, 582, L21
Baumgardt, H., Makino, J., Hut, P., & Portegies Zwart, S. 2003b, ApJ, 589, L25
Baumgardt, H, Makino, J., & Hut, P. 2005, ApJ, 620, 238
Bender, R., Saglia, R.P., & Gerhard, O.E. 1994, MNRAS, 269, 785
Binney, J., & Mamon, G.A. 1982, MNRAS, 200, 361
Cappellari, M., et al. 2002, ApJ, 578, 787
de Zeeuw, T., van den Bosch, R., Gebhardt, K. & Noyola, E. 2005, ApJ, submitted
Djorgovski, S. G., Gal, R. R., McCarthy, J. K., Cohen, J. G., de Carvalho, R. R., Meylan, G., Bendinelli, O., & Parmeggiani, G. 1997, ApJ, 474, L19
Dull, J.D., et al. 1997, ApJ, 481, 267
Fabian, A. 1999, MNRAS, 308, L39
Ferguson, A. M. N., Irwin, M. J., Ibata, R. A., Lewis, G. F., & Tanvir, N. R. 2002, AJ, 124, 1452
Ferguson, A., et al. 2005, ApJ, 622, L109
Ferrarese, L., & Merritt, D. 2000, ApJ, 539, L9
Filippenko, A., & Ho, L.C. 2003, ApJ, 588, L13
Fregeau, J.M., Gurkan, M.A., Joshi, K.J., & Rasio, F.A. 2003, ApJ, 593, 772
Foschini, L., et al. 2002, A&A, 392, 817
Gebhardt, K., & Fischer, P. 1995, AJ, 109, 209
Gebhardt, K., Richstone, D., Ajhar, E. A., Kormendy, J., Dressler, A., Faber, S. M., Grillmair, C., & Tremaine, S. 1996, AJ, 112, 105
Gebhardt, K., Rich, R.M.R., & Ho, L.C. 2002, ApJ, 578, L41
Gebhardt, K., et al. 2000a, ApJ, 539, L13
Gebhardt, K., et al. 2000b, ApJ, 543, L5
Gebhardt, K., et al. 2000c, AJ, 119, 1157
Gebhardt, K., et al. 2001, AJ, 122, 2469
Gebhardt, K., et al. 2003, ApJ, 583, 92
Gebhardt, K. 2004, in Carnegie Observatories Astrophysics Series, Vol. 1: Coevolution of Black Holes and Galaxies, ed. L. C. Ho (Cambridge: Cambridge Univ. Press), 249
Gerssen, J., van der Marel, R.P., Gebhardt, K., Guhathakurta, R., Peterson, R., & Pryor, C. 2002, AJ, 124, 3270; addendum 2003, AJ, 125, 376
Greene, J.E., & Ho, L.C. 2004, ApJ, 610, 722
Heinke, C.O. et al. 2005, ApJ, 625, 796
Ho, L. C. 1999, in Observational Evidence for Black Holes in the Universe, ed. S. K. Chakrabarti (Dordrecht: Kluwer), 157

Hurley, J., Pols, O., & Tout, C. 2000, MNRAS, 315, 543
Ibata, R., Chapman, S., Ferguson, A., Lewis, G., Irwin, M., & Tanvir, N. 2005, ApJ, submitted (astro-ph/0504164)
Jeffries, R.D. 1997, MNRAS, 288, 585
Kalirai, J., Richer, H., Hansen, B., Reizel, D., & Rich, R.M. 2005, ApJ, 618, L129
King, A., Davies, M., Ward, M., Fabbiano, G., & Elvis, M. 2001, ApJ, 552, L109
Kong, A., Rupen, M., Sjouwerman, L., & DiStefano, R. 2005, in "Relativistic Astrophysics: 22nd Texas Symposium" (astro-ph/0503465)
Kormendy, J., & Gebhardt, K. 2001, in The 20th Texas Symposium on Relativistic Astrophysics, ed. H. Martel & J. C. Wheeler (Melville: AIP), 363
Kormendy, J., & Richstone, D. 1995, ARA&A, 33, 581
Krajnovic, D., et al. 2005, MNRAS, 357, 1113
Lucy, L.B. 1974, AJ, 79, 745
Magorrian, J., et al. 1998, AJ, 115, 2285
Martini, P., & Ho, L. C. 2004, ApJ, 610, 233
Meylan, G., Sarajedini, A., Jablonka, P., Djorgovski, S. G., Bridges, T., & Rich, R. M. 2001, AJ, 122, 830
Murray, N., Quataert, E., & Thompson, T. 2005, ApJ, 618, 569
Pfahl, E., Rappaport, S., & Podsiadlowski, P. 2002, ApJ, 573, 283
Pinkney, J., et al. 2003, ApJ, 596, 903
Reitzel, D., Guhathakurta, P., & Rich, R.M. 2004, AJ, 127, 2133
Richstone, D., et al. 2005, ApJ, submitted (astro-ph/0403257)
Silk, J., & Rees, M. J 1998, A&A, 331, L1
Springel, V., Di Matteo, T., & Hernquist, L. 2005, ApJ, 620, L79
Thomas, J., et al. 2004, MNRAS, 353, 391
Tonry, J.L. 1983, ApJ, 266, 58
Tremaine, S., et al. 2002, ApJ, 574, 740
van de Ven, G., Verolme, E., Cappellari, M., & de Zeeuw, P. T. 2004, in IAU Symp. 220, Dark Matter in Galaxies, ed. S. D. Ryder et al. (San Francisco: ASP), 179
van der Marel, R.P. 1991, MNRAS, 253, 710
van der Marel, R.P. 1994, MNRAS, 270, 271
van der Marel, R.P. & Franx, M. 1993, ApJ, 407, 525
van der Marel, R.P., Gerssen, J., Guhathakurta, R., Peterson, R., & Gebhardt, K. 2002, AJ, 124, 3255
Wahba, G. 1990, Spline Models for Observational Data (Philadelphia: SIAM)
Weidemann, V. 2000, A&A, 363, 647
Zezas, A. L., & Fabbiano, G. 2002, ApJ, 577, 726

TABLE 1

KINEMATIC DATA FOR G1

Radius "	Velocity km s^{-1}	σ km s^{-1}	H3	H4
STIS data				
0.00	0.1 ± 1.3	31.1 ± 1.7	-0.02 ± 0.03	-0.07 ± 0.02
0.05	-0.4 ± 1.1	29.9 ± 1.4	0.04 ± 0.05	-0.02 ± 0.03
0.10	1.4 ± 1.1	29.5 ± 1.5	-0.01 ± 0.04	-0.02 ± 0.02
0.17	5.5 ± 1.1	26.9 ± 1.4	0.03 ± 0.04	-0.09 ± 0.01
0.30	4.6 ± 1.6	25.1 ± 1.5	0.04 ± 0.03	-0.05 ± 0.01
0.57	4.4 ± 2.3	25.3 ± 2.5	-0.01 ± 0.05	-0.06 ± 0.02
Keck/HIRES data				
0.00	0.2 ± 0.4	26.8 ± 0.7	0.04 ± 0.03	-0.10 ± 0.01
0.57	5.2 ± 0.2	26.7 ± 0.3	0.03 ± 0.01	-0.07 ± 0.01
1.34	12.1 ± 0.5	22.9 ± 1.3	-0.04 ± 0.03	-0.02 ± 0.02
2.30	12.5 ± 0.5	20.3 ± 0.6	-0.10 ± 0.02	0.00 ± 0.01
3.83	13.3 ± 1.7	18.9 ± 1.7	0.13 ± 0.06	0.09 ± 0.03